



Analysis of the pore structure characteristics of freeze-thawed saline soil with different salinities based on mercury intrusion porosimetry

Jiaqi Wang¹ · Qing Wang¹ · Yuanyuan Kong² · Yan Han¹ · Shukai Cheng¹

Received: 15 June 2019 / Accepted: 17 March 2020 / Published online: 30 March 2020
© Springer-Verlag GmbH Germany, part of Springer Nature 2020

Abstract

The pore structure characteristics of soil are closely related to soil engineering properties. For saline soil distributed in seasonally frozen areas, existing studies have focused on the influence of freeze–thaw cycles on pore structure, while the influence of soluble salt in the soil is not well understood. This study aims to explore the influence of salt content and salt type on the pore structure of freeze-thawed soil. Soil samples with different salt contents (0–2%) and types (bicarbonate salt and sulfate salt) were subjected to 10 freeze–thaw tests, and their pore size distributions (PSDs) were obtained by mercury intrusion porosimetry tests. In addition, the PSDs were quantitatively analyzed by fractal theory. For both salts, the PSDs of the tested soil samples were bimodal after the freeze–thaw cycles, and the porosity of saline soil samples increased with increasing salt content overall. However, the contents of various types of pores in soil samples with two salt types were quite different. The variation in bicarbonate salt content mainly affected the mesopore and macropore contents in the soil samples, and their change trends were opposite to each other. For soil samples with sulfate salt, the porosity and macropore content increased significantly when the salt content exceeded 1%. In addition, the pore structures in saline soil presented fractal characteristics after the freeze–thaw cycles, and the fractal dimension was positively correlated with macropore content. This study may provide references for understanding the engineering properties of saline soil in seasonally frozen areas at the microscale.

Keywords Salinized soil · Seasonally frozen region · Salt content · Salt type · Pore size distribution · Fractal dimension

Introduction

The macroscopic properties of soil, such as the mechanical and hydraulic properties, are controlled by its microstructure (Dalla Santa et al. 2019; Delage et al. 2006; Jiang et al. 2014; Terzaghi and Peck 1996; Zhang et al. 2018). In seasonally frozen soil areas, the soil experiences repeated freeze–thaw cycles due to temperature changes. When the temperature decreases, the liquid water in the soil gradually transforms into solid ice; when the temperature increases, the ice melts into water again. Moreover, freeze–thaw cycles weaken the soil structure and destroy the bonding force between the soil particles, leading to soil particle rearrangement (Konrad 1989; Wang et al. 2013). In recent years,

researchers have studied the microstructural characteristics of loess, soft soil, and silty clay under freeze–thaw cycles (Cui et al. 2014; Oztas and Fayetorbay 2003; Zhang and Cui 2017). The results showed that repeated freeze–thaw cycles significantly change the soil microstructure, which affects its engineering properties.

Saline soil is a special soil with a total content of soluble salt higher than 0.3% (Xiao et al. 2017), and it is widely distributed throughout the world. In seasonally frozen regions, the freezing process of saline soil is complicated due to the existence of soluble salt in the pore solution (Bing et al. 2007). Many studies have been performed on the engineering properties and microstructure of saline soil in seasonally frozen areas. Wang et al. (2018) studied the pore size distribution (PSD) of saline soil samples subjected to different numbers of freeze–thaw cycles and found that an increase in the number of freeze–thaw cycles mainly changes the macropore and mesopore contents in the soil, and their change trends are opposite to each other. The types of pores in soil samples are determined based on the pore diameter. Mesopores are pores with a diameter between 0.4

✉ Qing Wang
wangqing@jlu.edu.cn

¹ College of Construction Engineering, Jilin University, Changchun 130026, People's Republic of China

² School of Highway, Chang'an University, Xi'an 710064, People's Republic of China

and 4 μm , and macropores are pores with a diameter greater than 4 μm . Han et al. (2018b) demonstrated that freeze–thaw cycles affect the shear properties of saline soil by changing its microstructure. Liu et al. (2019b) showed that the porosity of lime-improved saline soils increased significantly after freeze–thaw cycles, which resulted in a decrease in the mechanical strength. These studies revealed that changes in the pore structure of saline soil are important factors for changes in the soil engineering properties. When the temperature drops below the freezing point of the pore water, the phase change of the pore water causes frost heaving in saline soil. In addition, the salt solubility decreases as the temperature decreases, and the salt in saline soil absorbs water and crystallizes from the pore solution; as a result, salt expansion occurs in saline soil due to the salt crystallization (Fang et al. 2018; Lai et al. 2016; Wan et al. 2017). Under these conditions, the pore structure characteristics of the soil change significantly. However, the existing studies on the pore structure of saline soil in seasonally frozen areas have focused on the influence of freeze–thaw cycles, while the influence of soluble salt in the soil is not well understood.

Bing et al. (2015) indicated that the water and salt in saline soil migrate and redistribute under repeated freeze–thaw cycles. Many studies have revealed that during the freezing process, saline soil has different freezing points and unfrozen water contents with variations in salt content and type (Bing and Ma 2011; Han et al. 2018a; Liu et al. 2018). Bing and He (2010) studied saline soil with different sodium sulfate contents and pointed out that the salt solubility varies with temperature during freeze–thaw cycles, and the soluble salt migrates with unfrozen water due to the temperature gradient. As a result, ice and salt crystals precipitate simultaneously, thus changing the pore structure of the soil (Xiao et al. 2018). Liu and Zhang (2014) indicated that the microstructure of saline soil varies with salt content and further determines its mechanical properties. You et al. (2017) indicated that the PSD of frozen silty clay changes with salt content. As the salt content increases, the porosity first increases and then decreases, and the turning point is at a salt content of approximately 1.5%. Therefore, under freeze–thaw cycle conditions, soluble salt is an important factor affecting the pore structure of saline soil. In seasonally frozen areas, the salt content in saline soil fluctuates with changes in the external environment. In addition, the salt type in the soil is multi-component rather than single component, which leads to a complicated phase-change process in saline soil. Therefore, studying the pore structure characteristics of saline soil with different salt contents and types under freeze–thaw cycles is of great practical significance.

The Songnen Plain in the northeast of China is a typical seasonally frozen area where a large area of saline soil is widely distributed; the soluble salt content in the soil is high (Zhang et al. 2017), the main salt type is bicarbonate salt,

and there is a certain amount of sulfate salt. Under these conditions, saline soil behaves as a structural soil; a large number of fissures often develop on the surface and inside of saline soil, leading to poor engineering properties and resulting in engineering hazards, such as slope instability and soil strength reduction. Therefore, studying the effects of the salt content and type on the pore structure characteristics of soil under freeze–thaw cycles can provide references for understanding the formation mechanism of fissure structures and the engineering properties of saline soil in seasonally frozen areas from a microscopic perspective.

The size and shape of the pores in the soil are complex, and the pore size covers multiple orders of magnitude, which makes it difficult to study them by the conventional geometric approaches. Therefore, many researchers have adopted fractal theory to study the pore structure of porous materials (Mahamud 2007; Ru et al. 2014; Wang et al. 2019). Fractal theory was proposed by Mandelbrot (1982) for studying irregular and complex phenomena and behaviors in nature, and has been widely used in many fields. Fractal theory is characterized by self-similarity and scale invariance; that is, there is similarity between a local area and the whole area of an object within a certain range of scales (Brakensiek et al. 1992; Mahamud and Novo 2008). Tyler and Wheatcraft (1989) first applied fractal theory to study the pore structure of soil and found that pores in soils have fractal characteristics with statistically self-similarity; they also found that fractal theory is suitable to study the pores in soil. In recent years, many researchers successfully analyzed the pore structure of different types of soil through fractal theory, such as loess, silty clay, and consolidated clay (Hu et al. 2014; Vallejo 1996; Zhang and Cui 2018), and the results proved that fractal theory is an effective method to study the pore structure of soil. The fractal dimension is an important parameter in fractal theory. The fractal dimension of pores indicates its irregularity and complexity. The larger the fractal dimension is, the more irregular the pore shape, the rougher the pore surface, and the more complicated the pore structure (Cui et al. 2015; Wang and Li 1997; Ye and Li 2019). In addition, the fractal dimension can well reflect pore structure changes in soil (Zhang and Cui 2017). Many researchers obtained pore fractal dimensions in porous materials through a combination of fractal models and microscopy tests, such as mercury intrusion porosimetry (MIP), N_2 adsorption, scanning electronic microscopy (SEM), nuclear magnetic resonance (NMR), and computed tomography (CT) (Cai et al. 2013; Li et al. 2019; Liu and Nie 2016). The MIP test is considered a reliable and effective method for the quantitative analysis of soil microstructure. The PSD characteristics of soil can be obtained by recording the mercury intrusion volume at each intrusion pressure (Sasanian and Newson 2013). In recent years, the MIP test has been successfully used by many researchers to study the

pore structure of soils (Ninjarav et al. 2007; Oualmakran et al. 2016; Shao et al. 2018). Chen et al. (2019) used three different fractal models to analyze the MIP data of loess and found that the pores in the loess have fractal characteristics of self-similarity within a pore size range of 3 nm–90 μm . Hu et al. (2014) drew similar conclusions by analyzing the fractal characteristics of loess before and after a stress path test. Therefore, we adopted the MIP test combined with fractal theory to analyze the pore structure of freeze-thawed saline soil in this study.

The purpose of this study, under the conditions of freeze–thaw cycles, was to explore (1) the PSDs of saline soil with different bicarbonate salt and sulfate salt contents; (2) the influences of bicarbonate salt and sulfate salt on the pore structure of soil; and (3) the fractal characteristics of the pores in saline soil with different salt contents and types. Two groups of remolded soil samples with different salt contents (0–2%) and salt types (NaHCO_3 and Na_2SO_4) were prepared for 10 freeze–thaw tests in a closed system. After the freeze–thaw tests, microscopic samples were taken from each soil sample for MIP tests to obtain their pore distributions, and fractal theory was used to quantitatively analyze the pores in soil samples. The variation in pore structure characteristics of freeze-thawed saline soil with the salt content and type was discussed.

Materials and methods

Soil properties

The tested saline soil was collected in Zhenlai County in Jilin Province of China, which is a typical seasonally frozen area. The undisturbed soil behaves as a structural soil in this region, and a large number of fissures and sand columns develop on the surface and inside of the soil (Fig. 1). The coordinate of the sampling point is N 45° 49' 41", E 123°

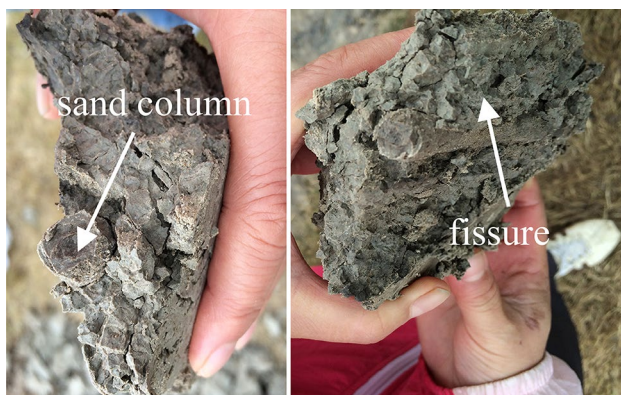


Fig. 1 Sand columns and fissures in undisturbed soil

13' 47", and the sampling depth is 20–50 cm, because the saline soil at this depth has the highest soluble salt content and is greatly affected by the change in external temperature. The collected disturbed soils were air-dried and mixed evenly in the laboratory for testing. The basic properties of the tested saline soil were obtained following the test procedure in GB/T50123–1999 (1999) by parallel testing. Tables 1 and 2 show the grain size distribution and mineralogical composition of the tested saline soil, respectively. The particle-size composition was determined by the densimeter and sieve method, and the mineral contents were tested by X-ray diffraction. The results show that the tested saline soil has a relatively high clay content, and the dominant mineral is quartz. According to the long-term observation data of the study area, western Jilin Province, the main cation in the saline soil is Na^+ , the main anions include HCO_3^- and SO_4^{2-} , and the content of other ions is very low (Han et al. 2018a, b; Wang et al. 2016; Zhang et al. 2019b, 2016). Therefore, we selected NaHCO_3 and Na_2SO_4 as the experimental focus in this study to investigate the effect of their contents on the pore structure characteristics of soil under freeze–thaw cycles. Table 3 shows the main physical and chemical properties of the tested saline soil and the corresponding test methods. The tested saline soil is a lean clay based on the USCS (ASTM 2011).

Sample preparation

Based on the chemical analysis results, two groups of remolded soil samples were prepared with different contents of NaHCO_3 and Na_2SO_4 for experiments. The long-term monitoring experimental data showed that the salt content in the saline soil varies with changes in the external environment, and the highest salt content can reach 1.54%. In addition, the boundary between saline soil and non-saline soil is 0.3%. Therefore, the salt contents selected in this study were 0%, 0.3%, 1%, 1.5%, and 2%. Note that the meaning of “%” here is the weight of salt as a percentage of the weight of dried saline soil. The saline soil collected for the

Table 1 Particle-size distribution of the tested saline soil

Particle size (mm)	> 2	2–0.075	0.075–0.005	0.005–0.002	< 0.002
Content (%)	0	8.4	47.0	3.7	40.9

Table 2 Mineral composition content of the tested saline soil

Relative contents of mineral (%)					
Quartz	Alkali feldspar	Plagioclase	Calcite	Dolomite	Kaolinite
49	15	25	6	3	2

Table 3 Physical and chemical properties of the tested saline soil

Property	Liquid limit (%)	Plastic limit (%)	Optimum water content (%)	Maximum dry density (g/cm ³)	Total salt content (%)	Na ⁺ (%)	HCO ₃ ⁻ (%)	SO ₄ ²⁻ (%)
Value	37.5	20.7	19.5	1.72	0.42	0.10	0.19	0.01
Method	Liquid-plastic limit joint determination method		Compaction test		Water-bath evaporation	Flame photometer	Neutralization titration	EDTA complex titration

Table 4 Salt contents and types of soil samples

Salt type	Salt content in soil (%)	Salt mass concentration in solution (%)
NaHCO ₃	0	0
	0.3	1.5
	1	4.9
	1.5	7.2
	2	9.5
Na ₂ SO ₄	0	0
	0.3	1.5
	1	4.9
	1.5	7.2
	2	9.5

Salt content in soil = $\frac{m_s}{m_s + m_d} \times 100\%$; Salt mass concentration in solution = $\frac{m_s}{m_s + m_w} \times 100\%$; where m_s , m_d , and m_w represent the weight of salt powder, dried soil, and water, respectively

test was first desalinated with distilled water, and then, the desalinated soil was crushed and passed through a 2 mm sieve after drying in an oven. Next, the sieved desalinated soil, distilled water, and salt powder (anhydrous NaHCO₃ and anhydrous Na₂SO₄) were mixed uniformly according to the calculated amount needed to obtain soil samples with different NaHCO₃ and Na₂SO₄ contents, as shown Table 4. The target water content of all soil samples was 19.5%. The soil samples were preserved in bags and sealed tightly for 24 h to allow an even distribution of water and salt. Then, the soil samples were transferred to a cylindrical mold and compacted into four layers according to a 90% degree of compaction on the basis of maximum dry density; the dry density of the remolded soil samples after compaction was 1.548 g/cm³. The remolded soil samples were covered by fresh-keeping films and stored in a moisturizing container to prevent the evaporation of water.

Freeze–thaw tests

In this study, freeze–thaw tests were performed in a closed system using a custom temperature-controllable freezing

device. The device can simulate a low-temperature environment with a minimum temperature of $-35\text{ }^\circ\text{C}$ and with a control accuracy of $0.1\text{ }^\circ\text{C}$. During the test, all soil samples were wrapped in fresh-keeping films with no external water supplement, and no loading was applied to the soil samples. First, soil columns with different salt contents wrapped with films were placed into a freezing chamber; the minimum temperature was set to $-30\text{ }^\circ\text{C}$, and the temperature was reduced by $4\text{ }^\circ\text{C}$ per hour. After freezing for 12 h, the soil columns were removed from the chamber and placed on a table to thaw for 12 h at room temperature. There was no external disturbance during the thawing process. The above process constituted a complete freeze–thaw cycle test, during which the water content of the soil columns remained unchanged due to the presence of the fresh-keeping film. Previous studies revealed that the structural and mechanical parameters of soils changed slightly after 5–10 freeze–thaw cycles (Liu et al. 2016; Xiao et al. 2014). Therefore, according to the above procedure, all soil columns were subjected to 10 freeze–thaw cycles in this study.

MIP tests

MIP tests were conducted on the soil samples after freeze–thaw cycles using an Autopore IV9500 mercury porosimeter (Micromeritics Instrument Corp.). The pore size measurement range of the instrument is $0.003\text{--}360.000\text{ }\mu\text{m}$. After the freeze–thaw tests, several cubic soil samples, each with a volume of approximately 1 cm^3 , were cut carefully from the center of each soil column group. Water can avoid crystallization and transform into nonexpanding amorphous ice when it is rapidly cooled at a low temperature below 136 K (Debenedetti 2003). Therefore, the soil samples were placed in liquid nitrogen ($-196\text{ }^\circ\text{C}$) immediately for freezing to convert the liquid water into nonexpanding amorphous ice. Then, the soil samples were removed and instantaneously placed into a freeze dryer (Beijing Boyikang Experimental Instrument Co. Ltd.) for vacuuming at $-50\text{ }^\circ\text{C}$ for 24 h to cause sublimation of the amorphous ice. Therefore, the dried soil samples were obtained without destroying the original structure. The freeze-dried soil samples were placed in a dilatometer and sealed after weighing; then, they were

loaded into a low-pressure chamber for analysis. After that, the dilatometer was weighed again and then loaded into a high-pressure chamber for analysis. During the test, the system automatically recorded the mercury intrusion volume at each intrusion pressure. According to the Washburn equation (Washburn 1921), the pores in soil are assumed to be cylindrical, and the relationship between the intrusion pressure P and the pore radius r is $P = -2\gamma \cos \theta / r$, where γ is the surface tension of the mercury (0.480 N/m at 20 °C) and θ is the contact angle (140°). For each salt content, at least two soil samples were tested to ensure the reliability of the experimental results, and the experimental data used in this paper are the mean values of the experimental results. The PSDs of soil samples with different salt contents and types after freeze–thaw cycles were obtained by MIP tests.

Results and discussion

Influence of the sodium bicarbonate content on the PSD

Figure 2 shows the PSDs of soil samples with sodium bicarbonate contents of 0%, 0.3%, 1%, 1.5%, and 2% after freeze–thaw cycles. The cumulative pore volume curve can reflect the porosity of each soil sample, and the pore diameters corresponding to the peak points in the pore size density curves are the most likely pore sizes, indicating that the content of pores with that size is the highest in soil samples.

Figure 2a shows that the shape of the curves was similar when the sodium bicarbonate content was less than 1%, and the slope of the curves changed at pore diameters of approximately 6 μm and 0.06 μm . The curves were flat when

the pore diameters were between 0.06 μm and 6 μm , which indicated that there was a high content of pores with diameters $> 6 \mu\text{m}$ and $< 0.06 \mu\text{m}$ in the soil samples when the salt content was less than 1%. When the sodium bicarbonate content reached 1%, the shape of the curves changed; the slope of the curves decreased when the pore diameters were $> 6 \mu\text{m}$, increased when the pore diameters were between 0.06 μm and 6 μm , and remained almost unchanged when the pore diameters were $< 0.06 \mu\text{m}$. Figure 2b shows that the PSD of the soil samples with different sodium bicarbonate contents after the freeze–thaw cycles were bimodal, in which the first peak was in the range of approximately 0.01–0.04 μm , and the second peak was in the range of approximately 1–40 μm with a larger distribution range. It is worth noting that the values of the two peaks of soil samples without salt were larger than those of the peaks of the soil samples containing sodium bicarbonate, indicating that the existence of sodium bicarbonate reduced micropore and macropore contents in the soil samples. As the sodium bicarbonate content increased, the change in the value and position of the first peak was not obvious, and the difference in the PSD was mainly in the range of the second peak.

Figure 2a shows that after experiencing the same number of freeze–thaw cycles, the total pore volume of the saline soil samples increased with increasing sodium bicarbonate content, increasing by approximately 18.2%, 23.2%, and 45.2% at salt contents of 1%, 1.5%, and 2%, respectively, compared to the soil sample with 0.3% salt content. The total pore volume of the soil samples with salt contents of 0% and 1.5% was almost identical; however, the difference in the PSD was obvious. To directly analyze the pore content in different ranges of pore diameter in each soil sample, the pores in soil are classified as micropores ($< 0.04 \mu\text{m}$), small

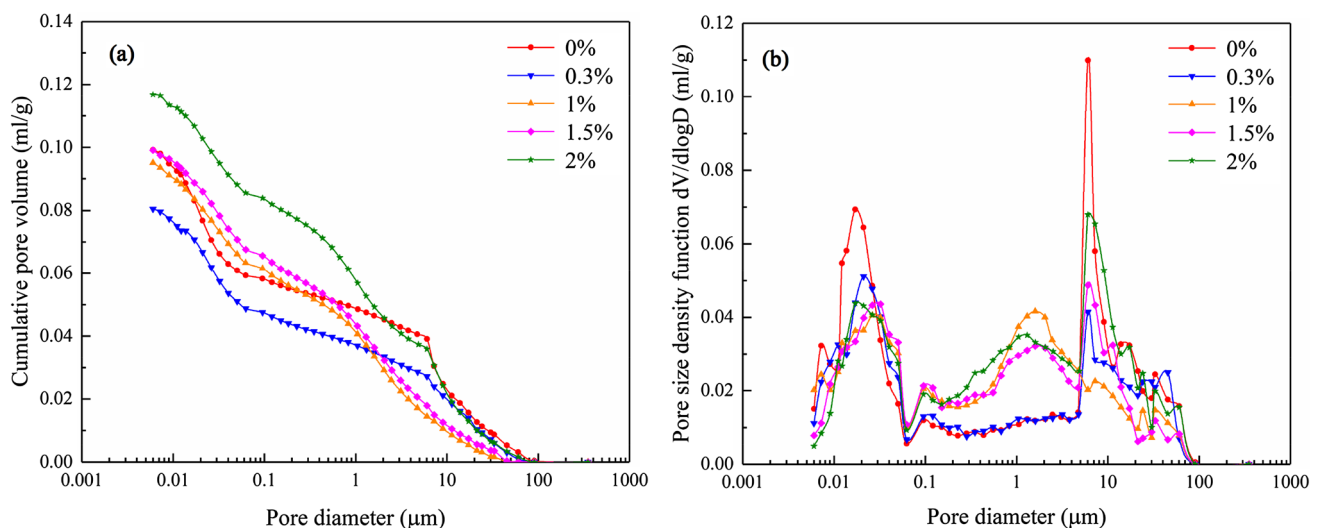


Fig. 2 PSDs of soil samples with different sodium bicarbonate contents: **a** cumulative pore volume curves; **b** pore size density function

pores (0.04–0.4 μm), mesopores (0.4–4 μm), and macropores (> 4 μm) according to (Wang and Wang 2000). Figure 3 presents the variation in the contents of different types of pores with sodium bicarbonate content. It can be seen that the micropore content showed a decreasing tendency, and the small pore content showed an increasing tendency overall with increasing sodium bicarbonate content; the change rate was relatively small. The contents of mesopores and macropores changed significantly with increasing sodium bicarbonate content.

Figure 3 shows that the content of macropores in the soil samples without salt was larger than that in the soil samples containing sodium bicarbonate. During the freezing process, the water freezes into ice completely in the soil sample without salt, resulting in a very low content of unfrozen water. A large displacement of soil particles occurred under the influence of frost heave. During the thawing process, the soil particles cannot return to the original position completely, leading to a high macropore content and a large total pore volume. It is worth noting that the mesopore content increased first and then decreased with increasing salt content with a turning point at a 1% salt content, while the macropore content showed the opposite tendency. This may be because frost heave is inhibited when the salt content is low (Bao et al. 2018). Therefore, the content of macropores in soil samples showed a decreasing tendency in the initial stage, while the variation trend changed when the content of salt exceeded 1%. In addition, the pore size distribution characteristics of soils are closely related to their particle-size distribution, and the existence of salt in the pore solution affects the particle size of the soil. The effect of the variation in salt concentration on the particle-size distribution of clay is generally explained by diffuse double-layer

theory (Chapman 1913; Gouy 1910). Clay particles usually carry a negative charge; when they interact with a pore solution, they attract cations, forming a diffuse double layer on the surface of the clay particles and creating a bound water film around the clay particles (Dolinar and Trauner 2007; Elkady and Al-Mahbashi 2017; Ye et al. 2014). The thickness of the diffuse double layer around the clay is affected by the cation valence and the ion concentration in the pore solution, and its thickness decreases with increasing ion concentration and cation valence (Mitchell and Soga 2005; Zhang et al. 2019a; Zhu et al. 2013). The freeze–thaw test is conducted in a closed system; thus, the water content of all the soil samples is the same. In addition, the cations in the pore solution of soil samples with different salt contents are all Na^+ . Therefore, the main factor affecting the thickness of the bound water film is the salt concentration. The thickness of the bound water film around the clay particles decreased with increasing salt concentration, and the distance between clay particles decreased, the force between the clay particles appeared as net attractive force, which resulted in an agglomeration of the clay particles (Deng et al. 2018; Zhang et al. 2013). The agglomeration effect of salt was relatively small when the salt concentration was low. Therefore, when the salt content was no higher than 1%, the micropore content decreased, while the contents of small pores and mesopores increased with increasing salt content. When the salt content was higher than 1%, the agglomeration effect of salt increased with increasing salt content, and fine particles further agglomerated into coarse particles. As a result, the macropore content increased, and the three other types of pores showed a similar decreasing tendency overall; the change rate in the macropore content was larger in the range of 1.5–2% salt content than at other salt contents. The

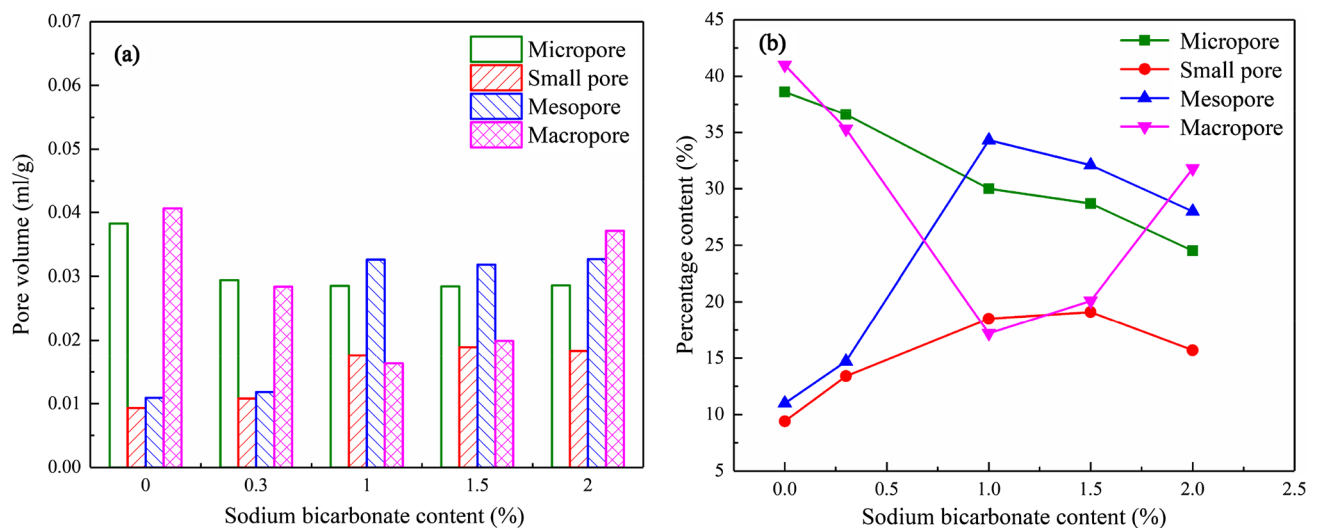


Fig. 3 Variation in the contents of different types of pores with sodium bicarbonate content: **a** pore volume content; **b** percentage content

migration of salt and water is a complicated process under freeze–thaw cycle conditions. The higher the salt content is, the more complicated this process. Therefore, the total pore volume of saline soil samples showed an increasing tendency with increasing sodium bicarbonate content after the freeze–thaw cycles.

Influence of the sodium sulfate content on the PSD

Figure 4 shows the PSDs of soil samples with different sodium sulfate contents after the freeze–thaw cycles. Figure 4a shows that the shape of the curves was similar when the sodium sulfate content did not exceed 1%. The slope of the curves also changed at pore diameters of approximately 6 μm and 0.06 μm; the curves were flat when the pore diameters were between 0.06 μm and 6 μm. The shape of the curves changed significantly when the sodium sulfate content exceeded 1% compared to the soil samples with different contents of sodium bicarbonate. The shape of the curves with pore diameters > 6 μm was steep, indicating that the pore content with pore diameters > 6 μm increased significantly when the sodium sulfate content exceeded 1%. Figure 4b shows that the PSDs of the soil samples with different sodium sulfate contents after the freeze–thaw cycles were bimodal. The value of the first peak was small, while the value and position of the second peak changed significantly with increasing sodium sulfate content. It is worth noting that the second peak gradually moved to the right when the salt content exceeded 1%; the peak values of the soil samples with salt contents of 1.5% and 2% increased by approximately three times compared with the soil sample without salt. The most likely pore sizes increased from 6.03 to 32.93 μm and 45.32 μm, respectively. The results demonstrated that under repeated freeze–thaw cycles, the

variation in sodium sulfate content significantly affected the macropore content in soil samples.

Figure 4a shows that the total pore volume of the soil samples showed an overall increasing tendency with increasing sodium sulfate content after the freeze–thaw cycles. The increase was most obvious in the soil samples with salt contents of 1.5% and 2%. Figure 5 presents the variation in the contents of different types of pores with sodium sulfate content. When the sodium sulfate content did not exceed 1%, micropores and macropores were the main pore types. With increasing sodium sulfate content, the change trend of various types of pores was similar to that of soil with sodium bicarbonate, i.e., the micropore and macropore contents showed a decreasing tendency, while the contents of small pores and mesopores showed an increasing tendency overall. This is because when the sodium sulfate content did not exceed 1%, it could completely dissolve in the pore water. According to diffuse double-layer theory, the thickness of the bound water film around the clay particles decreased with increasing salt content, which improved the attraction between the clay particles, resulting in an agglomeration of the clay particles. Therefore, the micropore content decreased, while the content of small pores and mesopores increased. When the salt content exceeded 1%, the micropore, small pore, and mesopore contents decreased with increasing sodium sulfate content; the macropore content increased significantly, and the change rate was the largest in the range of 1–1.5% sodium sulfate content compared with the other content levels. Except for the macropore content, the contents of the three other types of pores were low. Figure 6 shows the phase diagram of the Na₂SO₄–H₂O system (Steiger and Asmussen 2008). The corresponding salt concentrations in the pore solution are 0.5 mol/kg and 0.7 mol/kg when the salt content of the soil samples is 1.5%

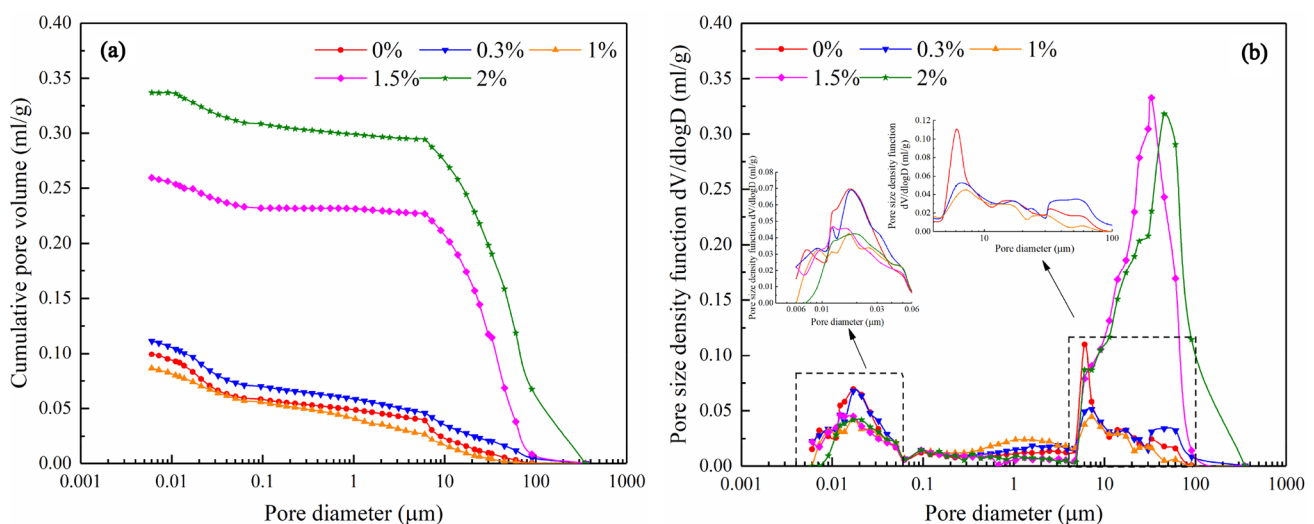


Fig. 4 PSDs of soil samples with different sodium sulfate contents: **a** cumulative pore volume curves; **b** pore size density function

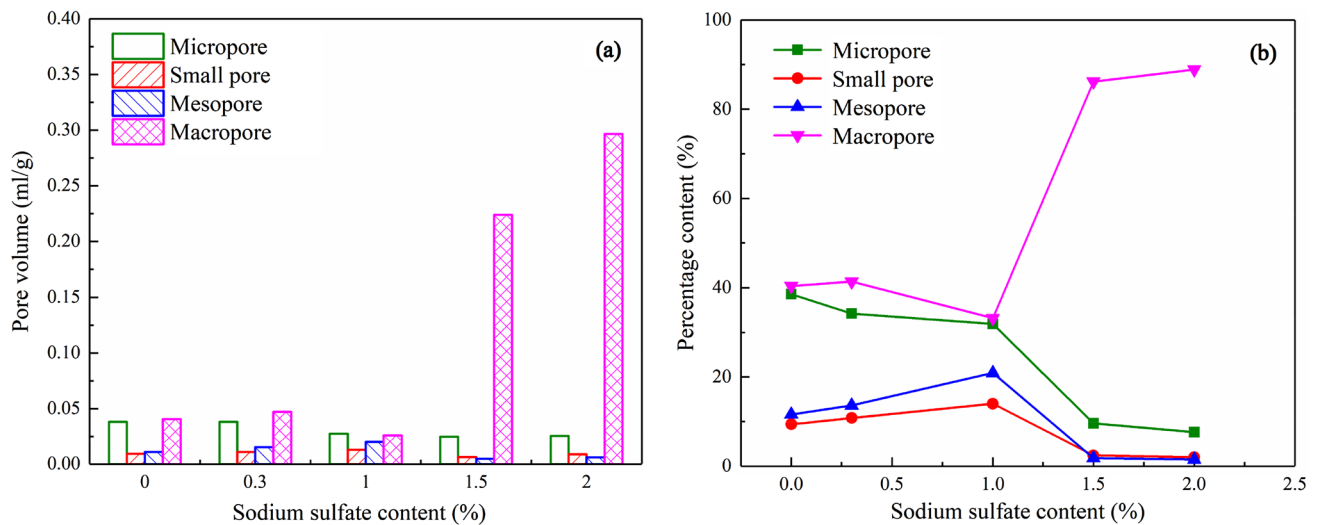


Fig. 5 Variation in the contents of different types of pores with sodium sulfate content: **a** pore volume content; **b** percentage content

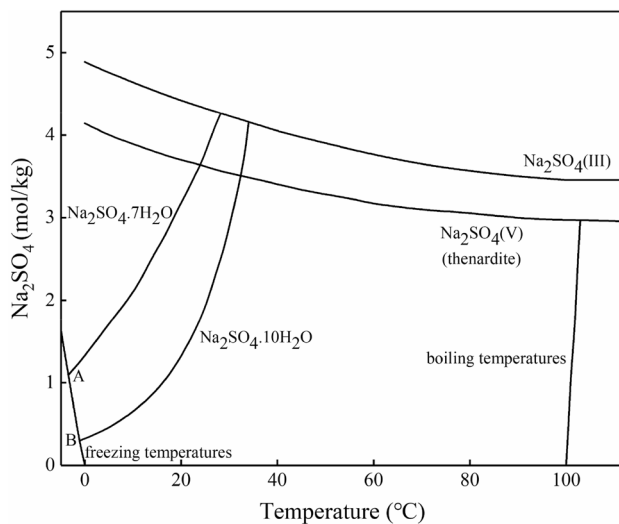


Fig. 6 Phase diagram of the $\text{Na}_2\text{SO}_4\text{-H}_2\text{O}$ system (Steiger and Asmussen 2008)

and 2%, respectively. It can be seen from the phase diagram that under these two salt concentrations, sodium sulfate combines with ten water molecules to form $\text{Na}_2\text{SO}_4 \cdot 10\text{H}_2\text{O}$ above 0 $^\circ\text{C}$, whose volume is 3.18 times higher than that of anhydrous sodium sulfate (Fang et al. 2018); the higher the salt content is, the higher the temperature at which the salt solution reaches saturation, and the more salt crystals will precipitate. The precipitation of mirabilite crystals generates a salt expansion force in the soil samples, and the salt expansion force increases with increasing crystallization, which results in the expansion and deformation of the soil samples (Lai et al. 2017; Wan et al. 2017). When the temperature drops below the freezing point of the pore water, the water

in the soil freezes to become ice, leading to frost heaving in the soil samples. Under the combined influence of the salt expansion force and frost heaving force, the compactness of soil samples decreased, and the structure loosened, which changed the PSD of the soil samples significantly under repeated freeze–thaw cycles. Therefore, when the sodium sulfate content exceeded 1%, the total pore volume and the content of macropores increased significantly with increasing sodium sulfate content under repeated freeze–thaw cycles.

Comparison of bicarbonate salt and sulfate salt

The above test results revealed that the salt type has a substantial influence on the pore structure of soil. A comparison of Figs. 2a and 4a suggests that the effects of salt contents less than 1% do not differ much with content or anion type. At 1.5% and 2.0% salt contents, sulfate increased the cumulative pore volume relative to that of bicarbonate by factors of 1.6 and 2.4, respectively, because the phase changes of the sodium bicarbonate and sodium sulfate solutions during the freezing process are different. Although, in the porous media of soil, the phase transition of the pore solution is not exactly the same as that of the free solution, the phase transition in the free solution can provide a reference for the phase transition in the pore solution to some extent (Xiao et al. 2017). The phase diagram of the $\text{Na}_2\text{SO}_4\text{-H}_2\text{O}$ system is shown in Fig. 6 in the previous section. Figure 7 shows the typical phase diagram of an inorganic aqueous binary system (Hasan et al. 2017; van der Ham et al. 1999), where the intersection of the ice line and the solubility line is called the eutectic point. The eutectic point of sodium bicarbonate is -2.23 $^\circ\text{C}$, and the corresponding salt mass concentration is

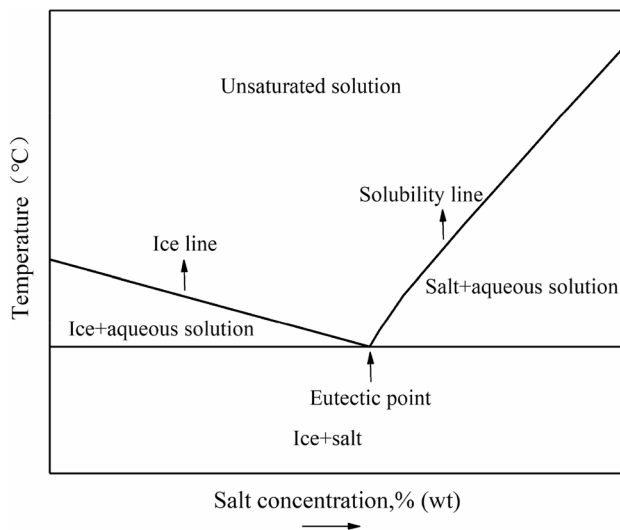


Fig. 7 Typical phase diagram of an inorganic aqueous binary system

6.27% (Hill and Bacon 1927; Pascual et al. 2010). The corresponding salt mass concentration in the pore solution is 1.5% and 4.9% when the salt content of the soil samples is 0.3% and 1%, respectively, and the pore solution concentration is less than the eutectic point concentration. It can be seen from the phase diagram that when the pore solution concentration is less than the eutectic point concentration, ice precipitated first as the temperature decreased. In this process, the pore solution concentration increased with decreasing liquid water content. When the solution concentration increased to the eutectic point concentration, salt crystallized from the pore solution. The effect of salt crystallization on the pore structure of the soil is not obvious, because the salt content is low. When the salt content of the soil samples is 1.5% and 2%, the corresponding salt mass concentration in the pore solution is 7.2% and 9.5%, respectively, and the pore solution concentration is larger than the eutectic point concentration. For both salts, the salt crystals precipitated as the solution reached saturation, which resulted in a decrease in the solution concentration. When the solution concentration decreased to the eutectic point concentration, ice crystals precipitated as the temperature continued to decrease.

For soil with sodium bicarbonate, the precipitated salt crystals are anhydrous NaHCO_3 , which has a needle-like shape with a very small size (Pascual et al. 2010). The change in pore structure of soil samples during the freeze–thaw cycle is mainly affected by frost heaving. For soil with sodium sulfate, Lai et al. (2016) indicated that when the salt content was less than 0.7%, salt crystallization almost did not occur in the soil, and when the salt content reached 1.5%, salt crystals precipitated from the pore solution before ice precipitated, resulting in salt expansion in the soil. According to the phase diagram of the $\text{Na}_2\text{SO}_4\text{-H}_2\text{O}$

system in the above section, the crystals that precipitated from the sodium sulfate solution have different types and states as the temperature decreases, such as heptahydrate ($\text{Na}_2\text{SO}_4\cdot 7\text{H}_2\text{O}$) and mirabilite ($\text{Na}_2\text{SO}_4\cdot 10\text{H}_2\text{O}$), both of which can generate crystallization pressure and cause salt expansion in porous materials (Steiger and Asmussen 2008). Figure 6 shows that the concentration corresponding to eutectic point A of the heptahydrate ($\text{Na}_2\text{SO}_4\cdot 7\text{H}_2\text{O}$) and ice is 1.096 mol/kg, and the corresponding salt content is 2.9%. The maximum salt content selected in this study is 2%, which is less than 2.9%. Therefore, the reason for the change in the soil pore structure is the salt expansion caused by the crystallization of mirabilite ($\text{Na}_2\text{SO}_4\cdot 10\text{H}_2\text{O}$). The corresponding salt concentrations in the pore solution are 0.5 mol/kg and 0.7 mol/kg when the salt content of the soil samples is 1.5% and 2%, respectively, which are higher than the concentration corresponding to eutectic point B in Fig. 6. Therefore, mirabilite ($\text{Na}_2\text{SO}_4\cdot 10\text{H}_2\text{O}$) can be formed at a positive temperature during the cooling process, and the volume is approximately three times higher than that of anhydrous sodium sulfate. The higher the initial salt concentration is, the more crystals precipitate, and the larger the salt expansion force. The soil structure became loose due to the combined action of salt expansion and frost heaving; as a result, the macropore content increased significantly. Therefore, the cumulative pore volume of soil samples with sulfate salt increased significantly compared to the soil sample with bicarbonate salt when the salt content was $> 1\%$. This suggested that sulfate salt had a greater influence than bicarbonate salt on the PSD of the soil under the freeze–thaw cycles.

Fractal analysis of the PSD

The commonly used fractal models for analyzing the MIP test data include the Menger model (Friesen and Mikula 1987), Neimark model (Neimark 1992), and thermal fractal model (Zhang and Li 1995; Zhang et al. 2006). Among them, the thermal fractal model has been successfully used by many researchers in different fields to analyze the pore structure of porous materials including soils (Tang et al. 2014; Yan et al. 2012; Yang et al. 2019; Zhang and Cui 2018). In addition, researchers have analyzed the pore structure of soil using different fractal models and have compared the analysis results. The results showed that the thermal fractal model is more accurate than other models and can obtain unique and reasonable fractal dimensions over the entire pore size range of soil (Hu et al. 2014; Huang et al. 2019; Liu et al. 2019a). Therefore, in this paper, the fractal characteristics of the PSD of freeze-thawed soil samples were analyzed using the thermal fractal model based on the experimental data obtained by MIP tests. This model is derived based on the principle of thermodynamics.

In the MIP test, the relationship between the intrusion pressure and intrusion volume can be expressed as follows:

$$\int_0^V P dV = - \int_0^S \gamma \cos \theta dS, \quad (1)$$

where P is the intrusion pressure; V is the mercury intrusion volume; γ is the surface tension of mercury; θ is the contact angle between mercury and the pore surface; and S is the pore surface area.

Equation (1) is equivalent to Eq. (2) (Zhang and Li 1995):

$$\sum_{i=1}^n \bar{P}_i \Delta V_i = k r_n^{2-D} V_n^{D/3}. \quad (2)$$

Equation (2) can be written in the form of Eq. (3):

$$\sum_{i=1}^n \bar{P}_i \Delta V_i = k r_n^2 (V_n^{1/3} / r_n)^D, \quad (3)$$

where \bar{P}_i denotes the average intrusion pressure for the i th time; ΔV_i denotes the mercury intrusion volume for the i th time; k is a constant; n is equal to the total intrusion segment number minus 1; and r_n and V_n denote the pore radius and the accumulated intrusion volume for n th times, respectively.

By designating:

$$W_n = \sum_{i=1}^n \bar{P}_i \Delta V_i, \quad (4)$$

$$Q_n = V_n^{1/3} / r_n. \quad (5)$$

Equation (3) can be expressed as:

$$\lg(W_n / r_n^2) = D \lg(Q_n) + C. \quad (6)$$

Taking $\lg(Q_n)$ as the abscissa and $\lg(W_n / r_n^2)$ as the ordinate, the slope of the curve denotes the thermal fractal dimension of the soil sample, where C is a constant.

Figures 8 and 9 show that there is an obvious linear relationship between $\lg(W_n / r_n^2)$ and $\lg(Q_n)$. All fitting coefficients reached 0.99, and the calculated fractal dimensions were all between 2 and 3, which demonstrated that this model is applicable for the tested soil samples (Zhang and Li 1995). Figure 10 presents the variation in the thermal fractal dimension of saline soil samples with salt contents and types after the freeze–thaw cycles. The results showed that the thermal fractal dimension of the soil samples with sulfate salt is larger compared to soil samples with bicarbonate salt. For the soil samples with bicarbonate salt, with increasing salt content, the thermal fractal dimension decreased first and then increased with a threshold salt content of approximately 1.22%, as shown in Fig. 10a. For the soil samples

with sulfate salt, the thermal fractal dimension showed an increasing trend with increasing salt content, and the change rate was the largest of the tested salt contents in the range of 1–1.5% salt content. Studies have shown that a larger fractal dimension of pores means a more complex pore structure, a rougher pore surface and a more irregular PSD in soil (Cui et al. 2015; Zhang and Cui 2017). As a quantitative parameter to express the pore structure, the fractal dimension of pores is related to the PSD and the pore volume content in different pore size ranges in porous materials (Ru et al. 2014; Wang et al. 2014; Zhang and Bing 2015; Zhou and Tang 2018). In addition, by comparing Fig. 10 with Figs. 3b and 5b, it was found that the change trend of the thermal fractal dimension and macropore content of soil samples with salt content is similar. Therefore, the fitted relationship between the thermal fractal dimension and the macropore content of the soil samples is shown in Fig. 11. The results showed that there is a positive correlation between the thermal fractal dimension and the macropore content. The larger the macropore content is, the larger the thermal fractal dimension. Zhou and Tang (2018) indicated that the surface structure of macropores is rougher than that of micropores. Therefore, with an increasing macropore content in soil, the pore distribution heterogeneity and the pore surface roughness increased; thus, the fractal dimension of soil pores increased. In other words, the pore size distribution varied with salt content and salt type, which resulted in a change in the fractal dimension of the pores in the soil samples.

Conclusions

MIP tests were performed to explore the pore structure of soil samples with different salt contents (0–2%) and salt types (NaHCO_3 and Na_2SO_4) after the samples experienced ten freeze–thaw cycles. The freeze–thaw tests were performed in a closed system. The results revealed that the PSDs of soil samples with different salt contents and types were all bimodal after the freeze–thaw cycles, and the porosity of saline soil samples increased with increasing salt content overall. However, the PSDs were quite different.

The variation in bicarbonate salt content mainly affected the mesopore and macropore contents in soil samples after the freeze–thaw cycles. The mesopore content increased first and then decreased with increasing salt content with a turning point at a 1% salt content, while the macropore content showed the opposite tendency. When the salt content exceeded 1%, fine particles agglomerated into coarser particles with increasing salt content, which increased the macropore content and decreased the contents of the other three types of pores overall. For soil samples with sulfate salt, the porosity and macropore content increased significantly when the salt content exceeded 1% under the

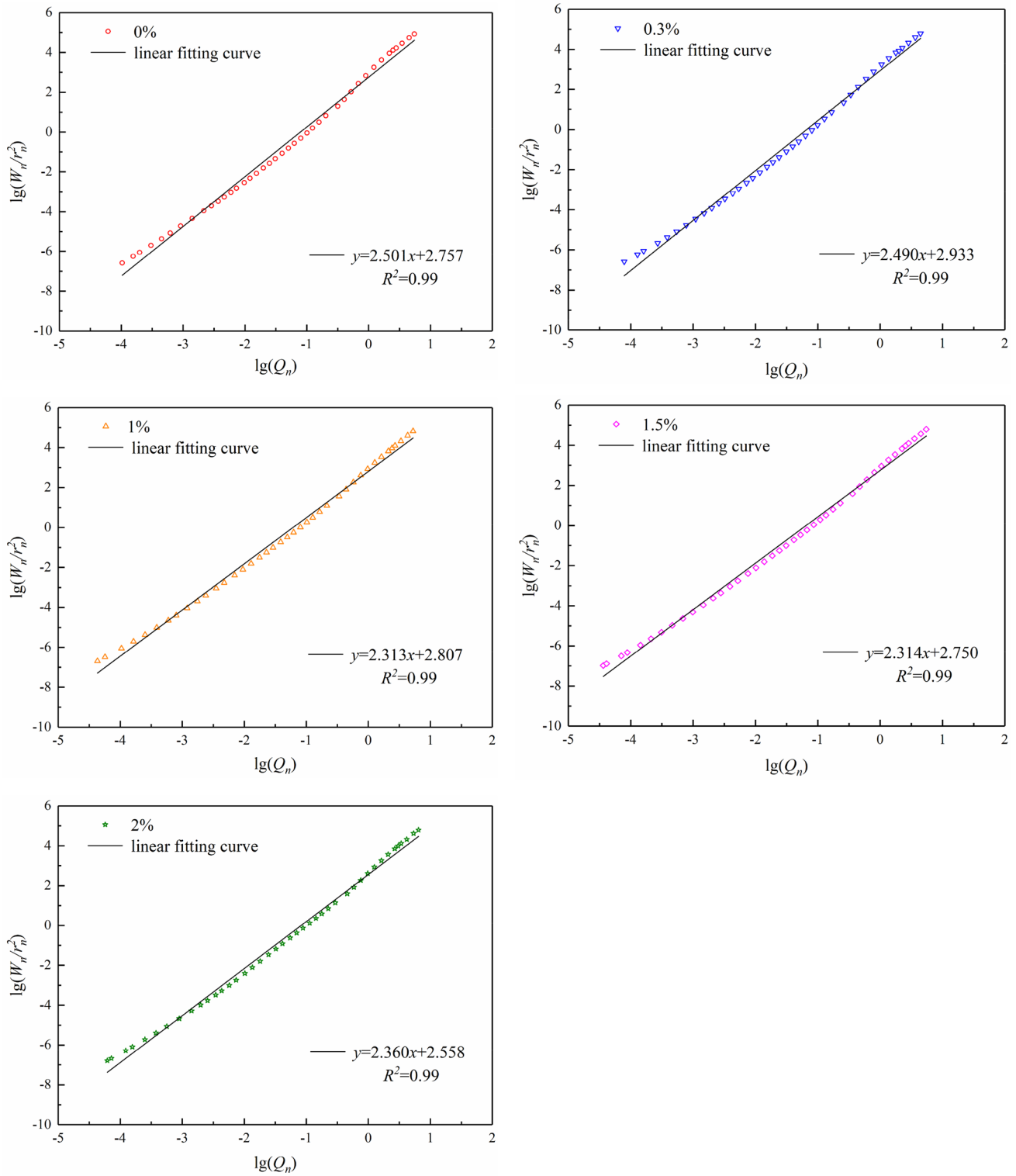


Fig. 8 Thermal fractal dimension of soil samples with different sodium bicarbonate contents

combined influence of salt expansion and frost heaving, and the change rate was the largest of the tested salt contents in the range of 1–1.5% salt content. At 1.5% and 2.0% salt

contents, sulfate increased the cumulative pore volume relative to that of bicarbonate by factors of 1.6 and 2.4, respectively. The essential reason for this result is that the phase

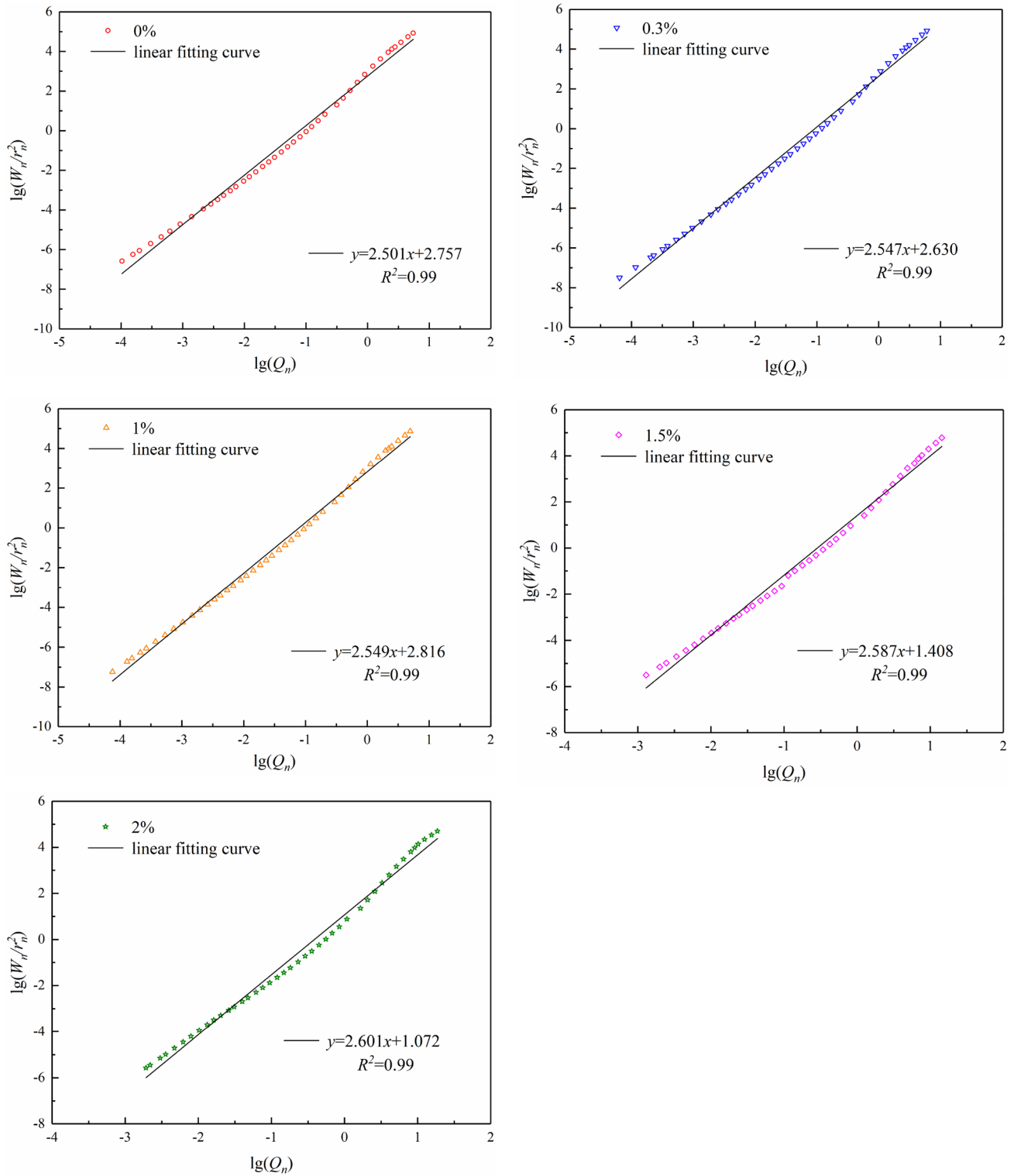


Fig. 9 Thermal fractal dimension of soil samples with different sodium sulfate contents

changes of these two salt solutions are different during the freezing process. In addition, the pore structures of saline soil samples presented fractal characteristics through fractal

analysis after the freeze–thaw cycles, and the fractal dimension was positively correlated with macropore content. The thermal fractal dimension of the sulfate saline soil was larger

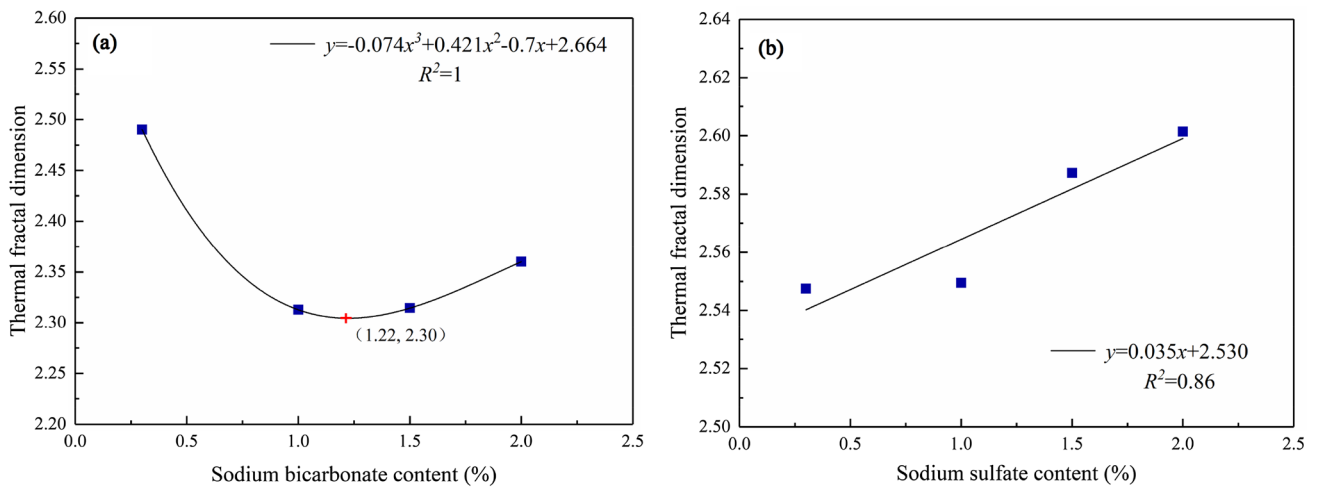


Fig. 10 Variation in thermal fractal dimension with salt content after freeze–thaw cycles: **a** sodium bicarbonate; **b** sodium sulfate

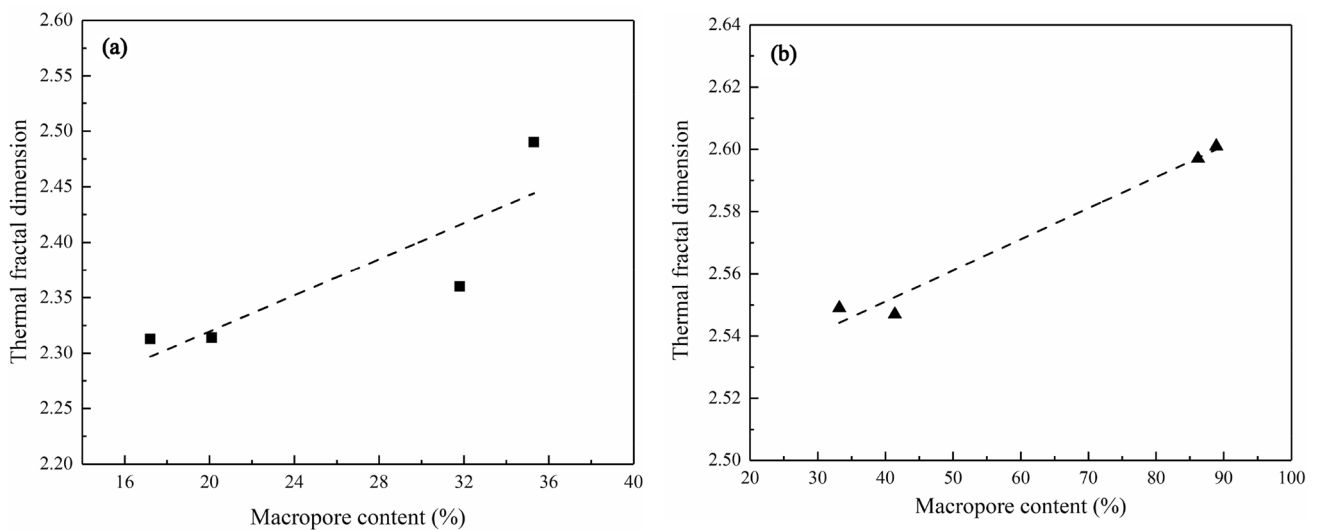


Fig. 11 Relationship between the thermal fractal dimension and macropore content of soil samples with **a** sodium bicarbonate; **b** sodium sulfate

than that of the bicarbonate saline soil, indicating that the PSD of the sulfate saline soil samples was more complex and that the sulfate salt had a greater influence than the bicarbonate salt on the PSD of the soil.

From the study, it can be seen that under freeze–thaw cycles, different salt contents and types had a substantial influence on the pore structure of soil, which further affected its macroscopic properties. The results may provide references for research on the engineering properties of saline soil in seasonally frozen areas at the microscale.

Acknowledgements This work was financially supported by the Key Project for International (Regional) Cooperation and Communication by the National Natural Science Foundation of China (Grant no.

41820104001), the State Key Program of the National Natural Science Foundation of China (Grant no. 41430642), and the Special Fund for Major Scientific Instruments of the National Natural Science Foundation of China (Grant no. 41627801). We sincerely thank the editors and all anonymous reviewers for their constructive and excellent reviews that helped to improve the manuscript.

References

- ASTM (2011) Standard practice for classification of soils for engineering purposes (unified soil classification system). D2487-11. ASTM International, West Conshohocken
- Bao S, Wang Q, Bian J (2018) Indoor frost heaving experiment of saline soil in Da’an area, Jilin Province. *J Eng Geol* 26:1701–1707

- Bing H, He P (2010) Experimental investigations on the influence of cyclical freezing and thawing on physical and mechanical properties of saline soil. *Environ Earth Sci* 64:431–436. <https://doi.org/10.1007/s12665-010-0858-y>
- Bing H, Ma W (2011) Laboratory investigation of the freezing point of saline soil. *Cold Regions Sci Technol* 67:79–88. <https://doi.org/10.1016/j.coldregions.2011.02.008>
- Bing H, He P, Yang C, Shi Y, Zhao S, Bian X (2007) Impact of sodium sulfate on soil frost heaving in an open system. *Appl Clay Sci* 35:189–193. <https://doi.org/10.1016/j.clay.2006.09.007>
- Bing H, He P, Zhang Y (2015) Cyclic freeze–thaw as a mechanism for water and salt migration in soil. *Environ Earth Sci* 74:675–681. <https://doi.org/10.1007/s12665-015-4072-9>
- Brakensiek DL, Rawls WJ, Logsdon SD, Edwards WM (1992) Fractal description of macroporosity. *Soil Sci Soc Am J* 56:1721–1723. <https://doi.org/10.2136/sssaj1992.03615995005600060010x>
- Cai Y, Liu D, Pan Z, Yao Y, Li J, Qiu Y (2013) Pore structure and its impact on CH₄ adsorption capacity and flow capability of bituminous and subbituminous coals from Northeast China. *Fuel* 103:258–268. <https://doi.org/10.1016/j.fuel.2012.06.055>
- Chapman DL (1913) LI. A contribution to the theory of electrocapilarity. *Lond Edinb Dublin Philos Mag J Sci* 25:475–481. <https://doi.org/10.1080/14786440408634187>
- Chen X, Zhang Z, Li D (2019) Study on the pore features of freezing–thawing loess based on different fractal models. *J Glaciol Geocryol* 41:1–11
- Cui Z-D, He P-P, Yang W-H (2014) Mechanical properties of a silty clay subjected to freezing–thawing. *Cold Reg Sci Technol* 98:26–34. <https://doi.org/10.1016/j.coldregions.2013.10.009>
- Cui Z-D, Zhao L-Z, Yuan L (2015) Microstructures of consolidated Kaolin clay at different depths in centrifuge model tests. *Carbon Evap* 31:47–60. <https://doi.org/10.1007/s13146-015-0252-7>
- Dalla Santa G, Cola S, Secco M, Tateo F, Sassi R, Galgaro A (2019) Multiscale analysis of freeze-thaw effects induced by ground heat exchangers on permeability of silty clays. *Geotechnique* 69:95–105. <https://doi.org/10.1680/jgeot.16.P.313>
- Debenedetti PG (2003) Supercooled and glassy water. *J Phys Condens Matter* 15:R1669–R1726. <https://doi.org/10.1088/0953-8984/15/45/r01>
- Delage P, Marcial D, Cui YJ, Ruiz X (2006) Ageing effects in a compacted bentonite: a microstructure approach. *Geotechnique* 56:291–304. <https://doi.org/10.1680/geot.2006.56.5.291>
- Deng Y, Zhang T, Cui Y, Chen Y, Deng T, Zhou X (2018) Pore water salinity effect on the intrinsic compression behaviour of artificial soft soils. *Appl Clay Sci* 166:299–306. <https://doi.org/10.1016/j.clay.2018.09.027>
- Dolinar B, Trauner L (2007) The impact of structure on the undrained shear strength of cohesive soils. *Eng Geol* 92:88–96. <https://doi.org/10.1016/j.enggeo.2007.04.003>
- Elkady TY, Al-Mahbashi AM (2017) Effect of solute concentration on the volume change and shear strength of compacted natural expansive clay. *Environ Earth Sci*. <https://doi.org/10.1007/s12665-017-6825-0>
- Fang J, Li X, Liu J, Liu C, Liu Z, Ji Y (2018) The crystallization and salt expansion characteristics of a silty clay. *Cold Reg Sci Technol* 154:63–73. <https://doi.org/10.1016/j.coldregions.2018.06.009>
- Friesen WI, Mikula RJ (1987) Fractal dimensions of coal particles. *J Colloid Interface Sci* 120:263–271. [https://doi.org/10.1016/0021-9797\(87\)90348-1](https://doi.org/10.1016/0021-9797(87)90348-1)
- GB/T50123–1999 (1999) Standard for soil test methods. China Planning Press, Beijing
- Gouy G (1910) Sur la constitution de la charge électrique à la surface d'un électrolyte. *J Phys (France)* 9:457–468
- Han Y, Wang Q, Kong Y, Cheng S, Wang J, Zhang X, Wang N (2018a) Experiments on the initial freezing point of dispersive saline soil. *CATENA* 171:681–690. <https://doi.org/10.1016/j.catena.2018.07.046>
- Han Y, Wang Q, Wang N, Wang J, Zhang X, Cheng S, Kong Y (2018b) Effect of freeze–thaw cycles on shear strength of saline soil. *Cold Reg Sci Technol* 154:42–53. <https://doi.org/10.1016/j.coldregions.2018.06.002>
- Hasan M, Filimonov R, Chivavava J, Sorvari J, Louhi-Kultanen M, Lewis AE (2017) Ice growth on the cooling surface in a jacketed and stirred eutectic freeze crystallizer of aqueous Na₂SO₄ solutions. *Sep Purif Technol* 175:512–526. <https://doi.org/10.1016/j.seppur.2016.10.014>
- Hill EA, Bacon LR (1927) Ternary systems. VI. Sodium carbonate, sodium bicarbonate and water. *J Am Chem Soc* 49:2487–2495
- Hu H, Jiang M, Peng J, Shen Z (2014) Pore fractal features of different kinds of loesses before and after stress path tests. *Rock Soil Mech* 35:2479–2485
- Huang H, An M, Wang Y, Yu Z, Ji W (2019) Effect of environmental thermal fatigue on concrete performance based on mesostructural and microstructural analyses. *Constr Build Mater* 207:450–462. <https://doi.org/10.1016/j.conbuildmat.2019.02.072>
- Jiang M, Zhang F, Hu H, Cui Y, Peng J (2014) Structural characterization of natural loess and remolded loess under triaxial tests. *Eng Geol* 181:249–260. <https://doi.org/10.1016/j.enggeo.2014.07.021>
- Konrad JM (1989) Physical processes during freeze–thaw cycles in clayey silts. *Cold Reg Sci Technol* 16:291–303
- Lai Y, Wan X, Zhang M (2016) An experimental study on the influence of cooling rates on salt expansion in sodium sulfate soils. *Cold Reg Sci Technol* 124:67–76. <https://doi.org/10.1016/j.coldregions.2015.12.014>
- Lai Y, Wu D, Zhang M (2017) Crystallization deformation of a saline soil during freezing and thawing processes. *Appl Therm Eng* 120:463–473. <https://doi.org/10.1016/j.appltherm.2017.04.011>
- Li X et al (2019) Heterogeneities of seepage pore and fracture of high volatile bituminous coal core: Implications on water invasion degree. *J Petrol Sci Eng* 183:106409. <https://doi.org/10.1016/j.petrol.2019.106409>
- Liu X, Nie B (2016) Fractal characteristics of coal samples utilizing image analysis and gas adsorption. *Fuel* 182:314–322. <https://doi.org/10.1016/j.fuel.2016.05.110>
- Liu J, Zhang L (2014) The Microstructure characters of saline soil in Qarhan Salt Lake area and its behaviors of mechanics and compressive strength. *Arab J Sci Eng* 39:8649–8658. <https://doi.org/10.1007/s13369-014-1410-2>
- Liu J, Chang D, Yu Q (2016) Influence of freeze–thaw cycles on mechanical properties of a silty sand. *Eng Geol* 210:23–32. <https://doi.org/10.1016/j.enggeo.2016.05.019>
- Liu L, Li Z, Liu X, Li Y (2018) Effect of salt content on freezing temperature and unconfined compression strength of lime-treated subgrade clay. *Appl Clay Sci* 158:65–71. <https://doi.org/10.1016/j.clay.2018.03.022>
- Liu P, Cui S, Li Z, Xu X, Guo C (2019a) Influence of surrounding rock temperature on mechanical property and pore structure of concrete for shotcrete use in a hot-dry environment of high-temperature geothermal tunnel. *Constr Build Mater* 207:329–337. <https://doi.org/10.1016/j.conbuildmat.2019.02.125>
- Liu Y et al (2019b) Experimental investigation of the geotechnical properties and microstructure of lime-stabilized saline soils under freeze–thaw cycling. *Cold Regions Sci Technol* 161:32–42. <https://doi.org/10.1016/j.coldregions.2019.03.003>
- Mahamud MM (2007) Textural changes during CO₂ activation of chars: a fractal approach. *Appl Surf Sci* 253:6019–6031. <https://doi.org/10.1016/j.apsusc.2006.12.109>
- Mahamud MM, Novo MF (2008) The use of fractal analysis in the textural characterization of coals. *Fuel* 87:222–231. <https://doi.org/10.1016/j.fuel.2007.04.020>

- Mandelbrot BB (1982) The fractal geometry of nature. Freeman, New York
- Mitchell JK, Soga K (2005) Fundamentals of soil behavior. Wiley, New York
- Neimark A (1992) A new approach to the determination of the surface fractal dimension of porous solids. *Phys A* 191:258–262. [https://doi.org/10.1016/0378-4371\(92\)90536-Y](https://doi.org/10.1016/0378-4371(92)90536-Y)
- Ninjarav E, Chung S-G, Jang W-Y, Ryu C-K (2007) Pore size distribution of pusan clay measured by mercury intrusion porosimetry. *KSCE J Civ Eng* 11:133–139
- Oualmakran M, Mercatoris BCN, Francois B (2016) Pore-size distribution of a compacted silty soil after compaction, saturation, and loading. *Can Geotech J* 53:1902–1909. <https://doi.org/10.1139/cgj-2016-0184>
- Oztaş T, Fayetorbay F (2003) Effect of freezing and thawing processes on soil aggregate stability. *CATENA* 52:1–8. [https://doi.org/10.1016/S0341-8162\(02\)00177-7](https://doi.org/10.1016/S0341-8162(02)00177-7)
- Pascual MR, Trambitas D, Calvo ES, Kramer H, Witkamp G-j (2010) Determination of the eutectic solubility lines of the ternary system $\text{NaHCO}_3\text{-Na}_2\text{CO}_3\text{-H}_2\text{O}$. *Chem Eng Res Des* 88:1365–1371. <https://doi.org/10.1016/j.cherd.2009.07.016>
- Ru J, Kong B, Zhu H, Shi Z, Zhang D, Fan T (2014) Microstructure, capillary performance and gas permeability of biporous copper fabricated by tape casting. *Powder Technol* 256:182–187. <https://doi.org/10.1016/j.powtec.2014.02.009>
- Sasanian S, Newson TA (2013) Use of mercury intrusion porosimetry for microstructural investigation of reconstituted clays at high water contents. *Eng Geol* 158:15–22. <https://doi.org/10.1016/j.enggeo.2013.03.002>
- Shao X, Zhang H, Tan Y (2018) Collapse behavior and microstructural alteration of remolded loess under graded wetting tests. *Eng Geol* 233:11–22. <https://doi.org/10.1016/j.enggeo.2017.11.025>
- Steiger M, Asmussen S (2008) Crystallization of sodium sulfate phases in porous materials: The phase diagram $\text{Na}_2\text{SO}_4\text{-H}_2\text{O}$ and the generation of stress. *Geochim Cosmochim Acta* 72:4291–4306. <https://doi.org/10.1016/j.gca.2008.05.053>
- Tang Y, Yang Q, Yu H (2014) Changes of the pore distribution of silty clay under the subway train loads. *Environ Earth Sci* 72:3099–3110. <https://doi.org/10.1007/s12665-014-3215-8>
- Terzaghi K, Peck RB (1996) Soil mechanics in engineering practice, 3rd edn. Wiley, New York
- Tyler SW, Wheatcraft SW (1989) Application of fractal mathematics to soil water retention estimation. *Soil Sci Soc Am J* 53:987–996. <https://doi.org/10.2136/sssaj1989.03615995005300040001x>
- van der Ham F, Witkamp GJ, de Graauw J, van Rosmalen GM (1999) Eutectic freeze crystallization simultaneous formation and separation of two solid phases. *J Cryst Growth* 198:744–748. [https://doi.org/10.1016/S0022-0248\(98\)01003-3](https://doi.org/10.1016/S0022-0248(98)01003-3)
- Vallejo LE (1996) Fractal analysis of the fabric changes in a consolidating clay. *Eng Geol* 43:281–290. [https://doi.org/10.1016/S0013-7952\(96\)00038-5](https://doi.org/10.1016/S0013-7952(96)00038-5)
- Wan X, Hu Q, Liao M (2017) Salt crystallization in cold sulfate saline soil. *Cold Reg Sci Technol* 137:36–47. <https://doi.org/10.1016/j.coldregions.2017.02.007>
- Wang F, Li S (1997) Determination of the surface fractal dimension for porous media by capillary condensation. *Ind Eng Chem Res* 36:1598–1602. <https://doi.org/10.1021/ie960555w>
- Wang Q, Wang J (2000) A Study on fractal of porosity in the soils. *Chin J Geotech Eng* 22:496–498
- Wang Q, Ma W, Zhang Z, Zhao S, Li G, Mao Y (2013) Research on the secondary collapse properties of loess under freeze-thaw cycle. *J Glaciol Geocryol* 35:376–382
- Wang X, Yao H, Li F, Zhang X, Yan J (2014) Fractal characterization of pore structure in coals based on thermodynamics model. *Coal Geol Explor* 42:20–23
- Wang N, Wang Q, Huo Z, Ma B, Chen Y (2016) Influence of salt and compaction on critical water content of frost heaving of saline soil. *J Eng Geol* 24:951–958
- Wang G, Wang Q, Zhang X, Wang W, Li C (2018) An experiment study of effects of freezing-thawing cycles on water and salt migration of saline soil. *Fresenius Environ Bull* 27:1060–1068
- Wang F, Yang K, You J, Lei X (2019) Analysis of pore size distribution and fractal dimension in tight sandstone with mercury intrusion porosimetry. *Res Phys* 13:102283. <https://doi.org/10.1016/j.rinp.2019.102283>
- Washburn EW (1921) Note on a method of determining the distribution of pore sizes in a porous material. *Proc Natl Acad Sci USA* 7:115–116. <https://doi.org/10.1073/pnas.7.4.115>
- Xiao D, Feng W, Zhang Z (2014) The changing rule of loess's porosity under freezing-thawing cycles. *J Glaciol Geocryol* 36:907–912
- Xiao Z, Lai Y, You Z, Zhang M (2017) The phase change process and properties of saline soil during cooling. *Arab J Sci Eng* 42:3923–3932. <https://doi.org/10.1007/s13369-017-2542-y>
- Xiao Z, Lai Y, Zhang M (2018) Study on the freezing temperature of saline soil. *Acta Geotech* 13:195–205. <https://doi.org/10.1007/s11440-017-0537-1>
- Yan C-L, Tang Y-Q, Liu Y-T (2012) Study on fractal dimensions of the silty soil around the tunnel under the subway loading in Shanghai. *Environ Earth Sci* 69:1529–1535. <https://doi.org/10.1007/s12665-012-1987-2>
- Yang J et al (2019) Segmented fractal pore structure covering nano- and micro-ranges in cementing composites produced with GGBS. *Constr Build Mater* 225:1170–1182. <https://doi.org/10.1016/j.conbuildmat.2019.08.016>
- Ye W, Li C (2019) The consequences of changes in the structure of loess as a result of cyclic freezing and thawing. *Bull Eng Geol Environ* 78:2125–2138. <https://doi.org/10.1007/s10064-018-1252-3>
- Ye WM, Zhang F, Chen B, Chen YG, Wang Q, Cui YJ (2014) Effects of salt solutions on the hydro-mechanical behavior of compacted GMZ01 Bentonite. *Environ Earth Sci* 72:2621–2630. <https://doi.org/10.1007/s12665-014-3169-x>
- You Z, Lai Y, Zhang M, Liu E (2017) Quantitative analysis for the effect of microstructure on the mechanical strength of frozen silty clay with different contents of sodium sulfate. *Environ Earth Sci*. <https://doi.org/10.1007/s12665-017-6454-7>
- Zhang Y, Bing H (2015) Experimental study of the effect of freezing-thawing cycles on porosity characters of silty clay by using mercury intrusion porosimetry. *J Glaciol Geocryol* 37:169–174
- Zhang Z-L, Cui Z-D (2017) Analysis of microscopic pore structures of the silty clay before and after freezing-thawing under the subway vibration loading. *Environ Earth Sci*. <https://doi.org/10.1007/s12665-017-6879-z>
- Zhang Z-L, Cui Z-D (2018) Effects of freezing-thawing and cyclic loading on pore size distribution of silty clay by mercury intrusion porosimetry. *Cold Reg Sci Technol* 145:185–196. <https://doi.org/10.1016/j.coldregions.2017.11.002>
- Zhang B, Li S (1995) Determination of the surface fractal dimension for porous media by mercury porosimetry. *Ind Eng Chem Res* 34:1383–1386. <https://doi.org/10.1021/ie00043a044>
- Zhang B, Liu W, Liu X (2006) Scale-dependent nature of the surface fractal dimension for bi- and multi-disperse porous solids by mercury porosimetry. *Appl Surf Sci* 253:1349–1355. <https://doi.org/10.1016/j.apsusc.2006.02.009>
- Zhang F, Wang G, Kamai T, Chen W, Zhang D, Yang J (2013) Undrained shear behavior of loess saturated with different concentrations of sodium chloride solution. *Eng Geol* 155:69–79. <https://doi.org/10.1016/j.enggeo.2012.12.018>
- Zhang X, Wang Q, Kong Y, Zhan J (2016) Study on physicochemical properties and water-salt movement law of saline soil in Nong' an County. *Yangtze River* 47:89–94

- Zhang X, Wang Q, Wang G, Wang W, Chen H, Zhang Z (2017) A study on the coupled model of hydrothermal-salt for saturated freezing salinized soil. *Math Probl Eng*. <https://doi.org/10.1155/2017/4918461>
- Zhang Y, Hu Z, Li L, Xue Z (2018) Improving the structure and mechanical properties of loess by acid solutions—an experimental study. *Eng Geol* 244:132–145. <https://doi.org/10.1016/j.enggeo.2018.07.023>
- Zhang T, Deng Y, Cui Y, Lan H, Zhang F, Zhang H (2019a) Porewater salinity effect on flocculation and desiccation cracking behaviour of kaolin and bentonite considering working condition. *Eng Geol* 251:11–23. <https://doi.org/10.1016/j.enggeo.2019.02.007>
- Zhang X et al (2019b) Experimental investigation of water migration characteristics for saline soil. *Pol J Environ Stud* 28:1495–1505. <https://doi.org/10.15244/pjoes/85952>
- Zhou J, Tang Y (2018) Experimental inference on dual-porosity aggravation of soft clay after freeze-thaw by fractal and probability analysis. *Cold Regions Sci Technol* 153:181–196. <https://doi.org/10.1016/j.coldregions.2018.06.001>
- Zhu C-M, Ye W-M, Chen Y-G, Chen B, Cui Y-J (2013) Influence of salt solutions on the swelling pressure and hydraulic conductivity of compacted GMZ01 bentonite. *Eng Geol* 166:74–80. <https://doi.org/10.1016/j.enggeo.2013.09.001>

Publisher's Note Springer Nature remains neutral with regard to jurisdictional claims in published maps and institutional affiliations.